Journal of Power Sources 227 (2013) 1–7

Contents lists available at SciVerse ScienceDirect

Journal of Power Sources

journal homepage: www.elsevier.com/locate/jpowsour

Supercapacitive performance of nitrogen-enriched carbons from carbonization of polyaniline/activated mesocarbon microbeads

Chun Wu, Xianyou Wang*, Bowei Ju, Lanlan Jiang, Hao Wu, Qinglan Zhao, Lanhua Yi

Key Laboratory of Environmentally Friendly Chemistry and Applications of Minister of Education, School of Chemistry, Xiangtan University, Hunan, Xiangtan 411105, China

HIGHLIGHTS

- The a-NENCs prepared by carbonizing PANI/ACMB and activated with 16 M HNO_3.
- The a-NENCs retain the leechee-like morphology of PANI/ACMB composites.
- Comparisons of NENCs and a-NENCs are carried out.
- The electrochemical properties of a-NENCs have been studied.

ARTICLE INFO

Article history:
Received 5 July 2012
Received in revised form
25 September 2012
Accepted 12 November 2012
Available online 20 November 2012

Keywords:
Polyaniline/activated mesocarbon microbeads
Carbonization
Nitrogen-enriched novel carbon material
Supercapacitive performances

ABSTRACT

With the direct carbonization using polyaniline/activated mesocarbon microbead (PANI/ACMB) composites as the precursor and subsequent activation treatment with 16 M HNO_3, the activated nitrogen-enriched novel carbons (a-NENCs) can be prepared. Scanning electron microscopy (SEM), Fourier infrared spectroscopy (FTIR), X-ray photoelectron spectroscopy (XPS) and nitrogen adsorption/desorption isotherm at 77 K are utilized to characterize the structure, morphology and physicochemical properties of the a-NENCs. The result shows that the a-NENCs keep the original leechee-like morphology of the PANI/ACMB composites. The supercapacitive performances of the a-NENCs are investigated with cyclic voltammetry (CV), galvanostatic charge/discharge tests, impedance spectroscopy (EIS) and cycle life measurements in 6 M KOH. The results based on galvanostatic charge/discharge tests demonstrate that the maximum specific capacitance of the a-NENCs electrode is 385 F g^{-1}. Meanwhile, the specific capacitance of the button supercapacitor using a-NENCs as electrode active material is as high as 89.5 F g^{-1} at the charge/discharge current density of 500 mA g^{-1}. These remarkable results demonstrate the exciting commercial potential for high performance, environmentally friendly and low-cost electrical energy-storage devices based on this new material.

1. Introduction

In recent years, supercapacitors have attracted considerable attention as alternative energy-storage systems. Various carbon materials including activated carbon [1,2], carbon aerogels [3] and mesoporous carbon [4] are the most frequently used electrode materials for supercapacitors because of their high surface area, good electronic conductivity and excellent stability [5,6]. The large specific surface area and high porosity of the activated carbon are the basic requirements to achieve the quick formation of a double-layer which results in a high power density and long durability of the supercapacitor, termed also electric double-layer capacitors (EDLC) [7]. However, the heteroatom and functional groups existed in a carbon matrix can significantly change the electron/donor characteristics of the carbon electrode material [8]. The oxygen-enriched surface groups, formed in most of the activated carbons during the activation process, have an acidic character, which could introduce electron-acceptor properties into the carbon surface. On the other hand, nitrogen-enriched functionalities have generally basic characters, inducing electron-donor properties [9]. The capacitive behavior of carbon materials can be further improved by the presence of active species that contribute to a fast and reversible Faradaic redox reaction, known as pseudocapacitance that generally derives from the Faradaic interactions between the ions of electrolytes and the carbon electrode surface [10].

The carbonization of conducting polymers, such as polyaniline (PANI), leads to a kind of materials, for example nitrogen-enriched carbon materials and oxygen-enriched carbon materials. The

* Corresponding author. Tel.: +86 731 58292060; fax: +86 732 58292061.
E-mail address: wxianyou@yahoo.com (X. Wang).

0378-7753/$ – see front matter © 2012 Elsevier B.V. All rights reserved.
http://dx.doi.org/10.1016/j.jpowsour.2012.11.028

nitrogen-enriched carbons can improve the wettability of carbon surface in the electrolyte and enhance the capacitance by additional Faradaic redox. Yuan et al. have synthesized the nitrogen-enriched carbon nanowires (NE-CNWs) from polyaniline (PANI) via a direct carbonization method. The specific capacitance of NE-CNWs-700 is as high as 327 F g^{-1} at 0.1 A g^{-1} [11]. Another report by Hulicova et al. describes the improvement of the supercapacitor behavior of melamine-based carbon synthesized by the direct carbonization of melamine and discusses the electrochemical performance of nitrogen-enriched carbons in aqueous and non-aqueous supercapacitors [12]. Usually, carbon materials can provide a limited EDLC, and conducting polymer can produce a large pseudocapacitance. Thus, the combination of EDLC and pseudocapacitance through coating conducting polymer on the surface of the carbon materials has extensively been applied in the field of supercapacitor. However, until recently, there is some lack of knowledge about the carbonization of carbon-conducting polymer composites and their application in supercapacitor. In this paper, the a-NENCs have been successfully prepared via a direct carbonization of the PANI/ACMB composites [13] and following activated by 16 M HNO_3. The aim of this work is to investigate the physical and electrochemical properties of the a-NENCs as a kind of electrode material in supercapacitors.

2. Experimental

2.1. Preparations of PANI/ACMB composites and a-NENCs

The PANI/ACMB composites were prepared using sodium dodecyl sulfate (SDBS) as the surfactant through chemical oxidation polymerization [14,15]. There were oxygen-enriched and nitrogen-enriched functionalities on the surface of the ACMB due to 16 M HNO_3 activation. These functional groups acted as anchor sites and enabled the subsequent in situ polymerization of PANI attaching on the surfaces of ACMB. Meanwhile, by introducing SDBS to the reaction system, which was hydrophilic and made the aniline monomers easily absorbed onto the surface of the ACMB. Besides, the π−π electron stacking interaction between the ACMB and the aniline was also beneficial to in situ polymerization occurring on the surface of ACMB. Therefore, the PANI would gradually grow along the initial nuclei of PANI and resulted in the extending growth of PANI [16]. To prepare the PANI/ACMB composites, the procedure was divided into two steps: (1) ACMB (0.1 g) and SDBS (0.2 g) were immersed in 1 M H_2SO_4 (15 mL) and kept for ultrasound about 10 min, 0.2 mL aniline was added to the above mentioned solution quickly with intensive stirring, then being stirred under 0 °C for 1 h; (2) Ammonium persulfate solution (the mass ratio of aniline/ammonium persulfate is 1:2.3) was added drop by drop to the solution mentioned in step 1, then the mixture was stirred at 0 °C for 6 h. The black-green product of the reaction was filtered and washed repeatedly with distilled water and alcohol. The resulting polymer was dried under vacuum at 70 °C for 12 h.

The as-prepared PANI/ACMB composites were carbonized under pure Ar atmosphere at 600 °C for 2 h to form nitrogen-enriched carbon materials named as NENCs. Finally, the resultant carbon was activated in 16 M HNO_3 at 70 °C for 24 h. The a-NENCs could be acquired after washed to be neutral and dried in oven at 100 °C. Fig. 1 shows a schematic mechanism of a-NENCs.

2.2. Preparation of the carbon sample electrodes

The supercapacitor electrodes materials were consisted of 80 wt % carbon sample, 10 wt% acetylene black, and 10 wt% polyvinylidene fluoride (PVDF) as usual. After well mixed, the mixtures were blended to obtain slurries. Then the slurries were coated on nickel foams that were used as current collectors and dried in vacuum overnight at 353 K. Finally, pressed the nickel foams under a pressure of 1.6×10^7 Pa. The geometric surface area of the electrodes was kept to be 1.0 cm^2.

2.3. Characterization of materials

To observe the transformation of the surface morphologies and microstructures between the PANI/ACMB composites and the a-

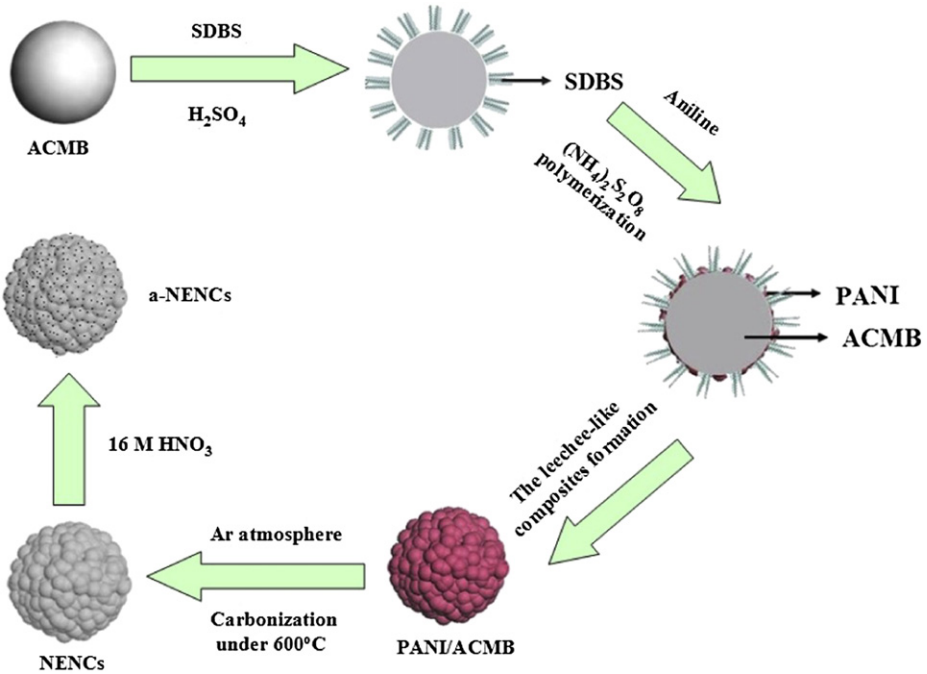

Fig. 1. A schematic mechanism of a-NENCs formation.

NENCs, the scanning electron microscopy (SEM) (JSE-6360LV) was used.

The FTIR measurement of the sample was characterized via a Fourier transform infrared (FTIR) spectrometer (Perkin–Elmer Spectrum One).

The surface characteristics of the nanocomposites were finished by X-ray photoelectron spectroscopy (XPS) (K-Alpha 1063, Thermo. Fisher Scientific, Britain).

The a-NENCs were examined by adsorption experiments of nitrogen, and adsorption/desorption isotherms of nitrogen were measured at 77 K on a Quantachrome autosorb automated gas sorption system. The estimation of Brunauer–Emmett–Teller (BET) specific surface area, pore volume and pore size distribution (PSD) were carried out according to the Brunauer–Emmett–Teller (BET) equation and Barrett–Joiner–Halenda (BJH) method.

2.4. Electrochemical measurements

The electrochemical behaviors of the NENCs and a-NENCs electrodes were performed by cyclic voltammetry, galvanostatic charge/discharge test and electrochemical impedance spectroscopy (EIS) conducted on a CHI660 (CH Instruments, USA) electrochemical workstation. The measurements were carried out in a standard three-electrode cell system, in which nickel and the Hg/HgO electrodes (SCE) were used as counter and reference electrodes, respectively. The voltage range for CV test varied from −1 to 0 V with the different scan rates of 1–10 mV s^{-1}. While, the voltage range for the galvanostatic measurement varied from 0 to 1 V at the current density from 1 to 5 A g^{-1}. The electrochemical impedance spectroscopy (EIS) in the frequency ranges from 10^5 Hz to 10^{-2} Hz with amplitude of 5 mV. Moreover, cycle life measurements were carried out by potentiostat/galvanostat (BTS 6.0, Neware, Guangdong, China) on button supercapacitor. The symmetrical button supercapacitors were assembled according to the order of electrode-separator-electrode. And all tests were impregnated in 6 M KOH electrolyte.

3. Results and discussion

3.1. Structure analysis

In order to fully carbonized PANI encapsulated on the surface of ACMB, the effects of carbonization temperature on the electrochemical performance of a-NENCs are studied. It has been found that the optimum carbonization temperature is 600 °C. Fig. 2 shows the SEM images of the PANI/ACMB composites and a-NENCs. It has been found from Fig. 2b that the a-NENCs with a diameter about 1 μm keep the original leechee-like morphology of PANI/ACMB composites after being carbonized at 600 °C. The external surface of the a-NENCs is coarse and porous due to 16 M HNO_3 activation. This kind of porous structure can significantly offer the quick transport channel of electrolyte ion, which could induce better electrochemical performance. So, it can be expected that the a-NENCs will provide a high specific capacitance and excellent electrochemical characteristics.

The FTIR spectrum of the a-NENCs (Fig. 3) show the disappearance of the characteristic peaks of the PANI/ACMB composites, which presented in the PANI/ACMB composites precursor at 1574.6 cm^{-1} (quinonoid (Q) ring stretching), 1492 cm^{-1} (benzenoid (B) ring stretching), 1281.1 cm^{-1} (the C–N stretching of secondary aromatic amine), 1121.7 cm^{-1} (the B-NH^+=Q stretching) and 823.3 cm^{-1} (aromatic C–H out-of-plane deformation vibration of 1,4-disubstituted benzene ring, γ (C–H), in linear PANI backbone) [17–19]. While, the peaks positioned at 1713.4 cm^{-1} in the IR spectrum of a-NENCs is clearly observed, which is attributed to the characteristic stretching vibration of C=O group due to 16 M HNO_3 activation. The peak at 1574.6 cm^{-1} is assigned to C=N stretching modes [20] mixed with aromatic C–C stretching vibrations [19] and quinonoid (Q) ring stretching, while the broad band centered at 1281.1 cm^{-1} corresponds to the vibrations of various C–N [21] and C–C bonds [22]. Therefore, there are a lot of nitrogen-enriched and oxygen-enriched groups on the surface of a-NENCs.

The XPS spectrum of the a-NENCs is illustrated in Fig. 4, which indicates the presence of three distinct peaks and can be explained by existence of carbon, nitrogen, and oxygen atoms. The Cls spectra of the samples have been resolved into three individual component peaks [23] representing graphitic carbon (peak 1, BE = 284.7), carbonyl group (peak 2, BE = 287.1) and carboxyl group (peak 3, BE = 289.5), respectively. The Ols spectra of the samples reveal the presence of three peaks [23,24] corresponding to carbonyl type groups and/or quinine (peak 1, BE = 531.0–531.1 eV), C–OH and/or C–O–C groups (peaks 2 and 3, BE = 532 and 532.4–533.1 eV), respectively. The chemical state of nitrogen atoms in carbonized samples could be assigned to four types according to previous reports [25,26]. These four types are indexed as following binding energies: pyridine-N-6 (peak 1, BE = 398.8 eV), pyrrole or pyridone-N-5 (peak 2, BE = 400.2 eV), quaternary-N-Q (peak 3, BE = 400.9 eV), chemisorbed nitrogen oxides-N-Ox (peak 4, BE = 405.8 eV). Meanwhile, the contents of C, N and O are 72.6%, 8.2% and 19.2%, respectively.

The N_2 adsorption/desorption isotherms and pore characteristics of PANI/ACMB composites and a-NENCs are compared in Fig. 5 and Table 1. For PANI/ACMB composites, a hysteresis loop is observed, thus indicating that the composite consists of micropore and mesopore. While the isotherm for a-NENCs is of type I according to IUPAC classification, indicating that the a-NENCs have the structure of microporous. The micropores participate in the charge/storage process of supercapacitors by providing abundant adsorbing sites for the ions [27]. And to some extent, the higher content of micropores, the higher capacitance values obtained [28].

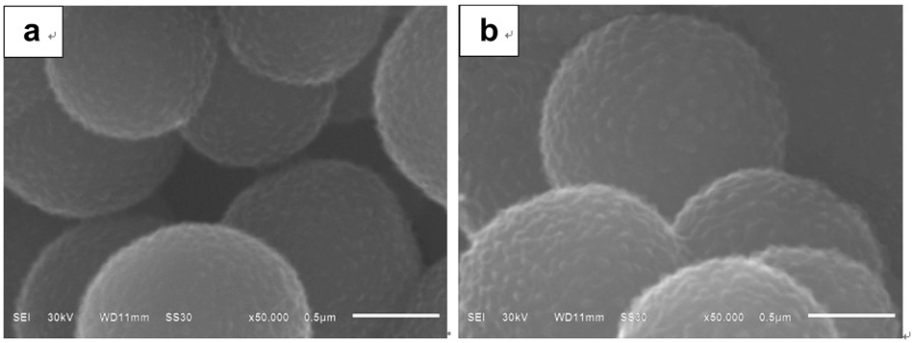

Fig. 2. SEM images of PANI/ACMB composites (a) and a-NENCs (b).

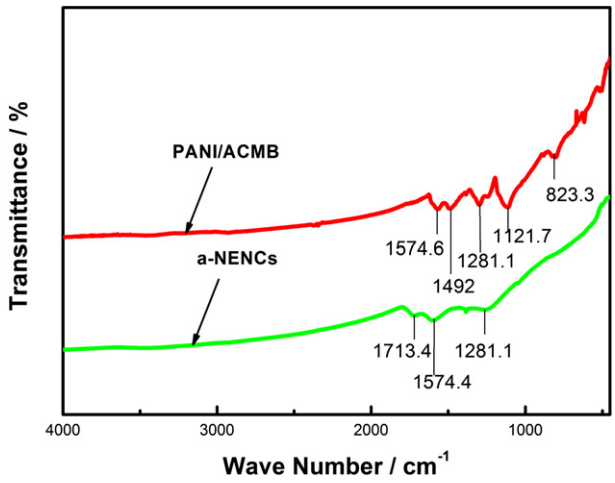

Fig. 3. FTIR spectra of PANI/ACMB composites and a-NENCs.

In addition, the adsorption and desorption branch is not closed at the low relative pressure, implying that an organic polymer framework of PANI is kept [29]. Meanwhile, as being seen from Table 1, the surface area of the a-NENCs is remarkably increased and possesses a high value of 420 $m^2\ g^{-1}$ compared to that of the PANI/ACMB composites (18.7 $m^2\ g^{-1}$), indicating the formation of many microprores [30].

3.2. Measurements of the electrochemical performance

To evaluate the electrochemical characteristics of the a-NENCs, the CV curves in 6 M KOH electrolyte are performed at the potential window from −1 to 0 V (vs. Hg/HgO) (Fig. 6). The CV curves for NENCs and a-NENCs at a scan rate of 10 mV s^{-1} are presented in Fig. 6a. Although there exist pseudocapacitive characteristics for NENCs and a-NENCs since both materials all derive from carbonization of ACMB/PANI composite, the area surrounded by CV curve of the a-NENCs is obviously larger than that of NENCs, which means that the capability of charge loading and releasing for a-NENCs is larger than NENCs due to the existence of a lot of micropores after activation treatment.

In addition, the effects of scan rates on the capacitive behavior of the a-NENCs are also investigated. Fig. 6b shows CV curves of a-NENCs at various scan rates. Notably, with the increase of the scan rate, the voltammetric curves deviate from rectangular shape, which is attributed to the presence of pseudocapacitive interactions between the positively charged ions. Furthermore, the small humps at −0.4 to −0.8 V are observed from the curves, which usually attributes to pseudo-Faradic reactions involving the quinone functional groups [28]. The main reason is that the nitrogen-enriched functionalities have generally basic characterization and form the active centers, inducing electron-donor properties. These electrochemically active centers contribute to the pseudcapacitance, which generally originates from the Faradaic interactions of the nitrogen atoms on carbon materials. The specific capacitance can be determined by Eq. (1) [31]:

$$C_{s,t} = \frac{I_a + |I_c|}{2W(dV/dt)} \quad (1)$$

where $C_{s,t}$, I_a, I_c, W and dV/dt are the specific capacitance (F g^{-1}), the current (A) of anodic and cathodic voltammetric curves on positive and negative sweeps, the mass of the material (g) (only including the mass of the a-NENCs, the same below), and the sweep rate

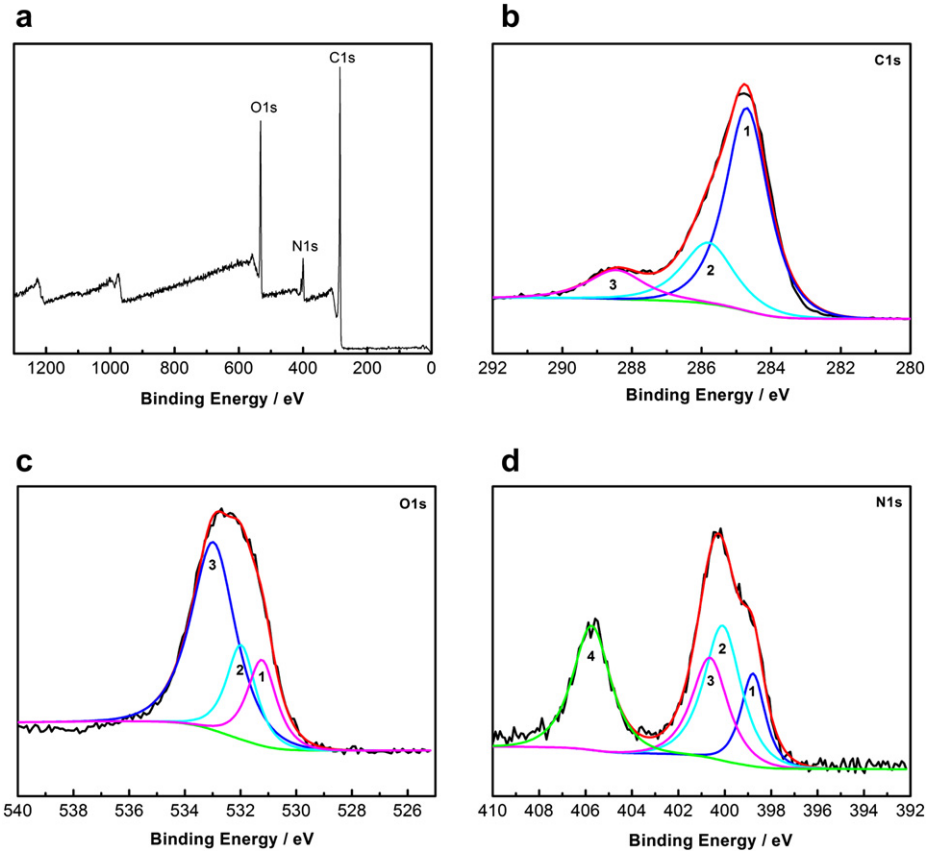

Fig. 4. X-ray photoelectron spectra of the a-NENCs: survey spectrum (a), C1s (b), O1s (c) and N1s (d).

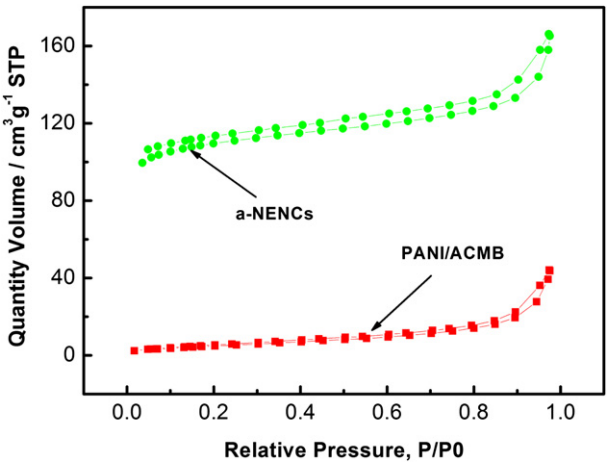

Fig. 5. Nitrogen adsorption/desorption isotherms of PANI/ACMB composites and a-NENCs.

(mV s^{-1}), respectively. It can be calculated from Eq. (1) that the specific capacitance can reach the maximum value of 366 F g^{-1} when the potential scan rate is equal to 1 mV s^{-1}. Especially, it can be noted from Fig. 6b that with the increase of the scan rate, the capacitance of the a-NENCs is slowly degraded. Even so, the specific capacitance is still about 279.3 F g^{-1} at the scan rate of 10 mV s^{-1}, thus indicating an excellent rate capability of the a-NENCs. Fig. 6c also shows the change of the specific capacitance retention with different scan rates. Obviously, with growth of scan rates from 1 mV s^{-1} to 10 mV s^{-1}, the retention of capacitance is all above 75%. This result shows that the a-NENCs have good rate capability, which is important for high power density.

Galvanostatic charge/discharge measurements have also been conducted in order to investigate the supercapacitive performance of the a-NENCs. In Fig. 7a shows the galvanostatic charge/discharge curves of the NENCs and a-NENCs at the current density of 1 A g^{-1}. It is obvious that the specific capacitance of a-NENCs electrode is more than that of NENCs, indicating that the a-NENCs possess a better capacitive behavior under this loading current density.

Furthermore, the galvanostatic charge/discharge curves of the a-NENCs at different current densities can be noted from Fig. 7b. The variations of the curves are not linear with the change of charge/discharge time and give rise to an inflexion, and this inflexion further verifies that the nitrogen-enriched group in the surface of the a-NENCs can offer a pseudocapacitance effect. And at the beginning of the discharge curves there are a few sudden potential drops (IR drop), which are attributed to the resistance of electrolytes and the resistance of ion diffusion in micropores [32]. Usually, IR drop is a direct measure of equivalent series resistance (ESR), which influences the overall power performance of a capacitor. In order to clearly calculate the IR value, the inset in Fig. 7 depicts the IR drops of the a-NENCs, which shows a very low value. Besides, it can be noted that the specific capacitance of the a-NENCs electrode decreases with the increasing of discharge current density, the reason is that the electrolyte ion cannot penetrate well into the inner of active materials due to slow diffusion at large current density. And the specific capacitance of a-NENCs is as high as

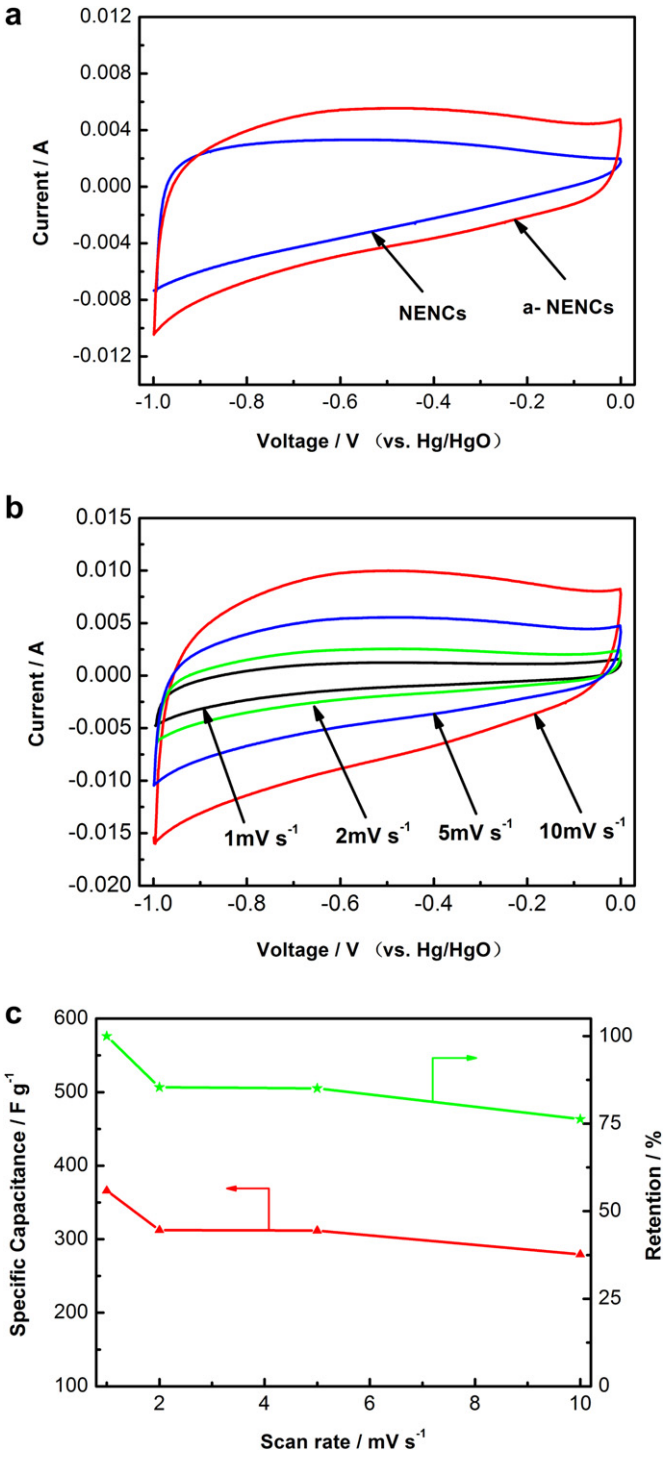

Fig. 6. (a) The CV curves of NENCs and a-NENCs at 10 mV s^{-1}, (b) The CV curves of the a-NENCs electrode at different scan rates and (c) The specific capacitance (-▲-) and retention (-★-) of the a-NENCs electrode at different scan rates.

Table 1
Pore characteristics of PANI/ACMB composites and a-NENCs.

	BET-SSA (m^2 g^{-1})	Average aperture (nm)	Pore volume (cm^3 g^{-1})
PANI/ACMB	18.7	1.65	0.076
a-NENCs	420	1.26	0.14

385 F g^{-1} at a current density of 1 A g^{-1}, which is higher than that of NE-CNWs-700 (327 F g^{-1} at 0.1 A g^{-1}) reported by Yuan et al. [11], that is, the specific capacitance of a-NENCs is larger than that of NE-CNWs-700 under the higher current density, indicating that the a-NENCs possess more excellent electrochemical performances. The specific capacitance can be evaluated from the slope of the charge/discharge curves, according to Eq. (2) [33]:

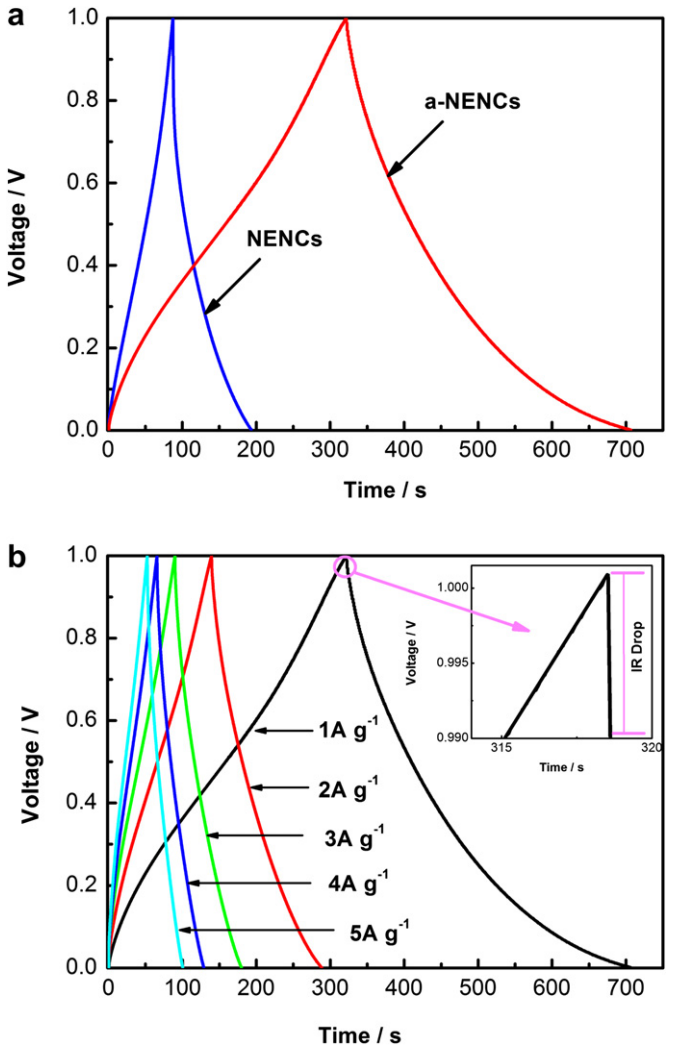

Fig. 7. (a) The galvanostatic charge/discharge curves of the NENCs and a-NENCs at the current density of 1 A g^{-1}, and (b) The galvanostatic charge/discharge curves of the a-NENCs at different current densities and the IR drop insert.

$$C_m = \frac{it}{m\Delta V} \quad (2)$$

Here, C_m is the specific capacitance (F g^{-1}), i is the charge/discharge current (A), ΔV is the potential range of the charge/discharge (V), t_d is the discharge time (s), and m is the mass of active material (g) within the electrode.

In order to further analyze the electrochemical properties about characteristic frequency responses of the electrode materials, EIS measurements are employed. Fig. 8 shows the ac impedance spectrum (Nyquist plots) responding to frequency for electrodes of the samples. It can be found that there is straight line in the low-frequency region (lower than 100 Hz) because of Warburg impedance, which is a result of the frequency dependence of ion diffusion in the electrolyte to the electrode interface [34–37]. Meanwhile, the straight line part of a-NENCs leans more toward the imaginary axis than the NENCs, and indicating a good capacitive behavior. Furthermore, the value of ESR, namely the equivalent series resistance consisting of electronic contributions and ionic contributions (the inset in Fig. 8), for a-NENCs is estimated around 0.93 Ω from the crossover point of the highest frequency with the real part of the impedance, lower than that of NENCs. Charge-

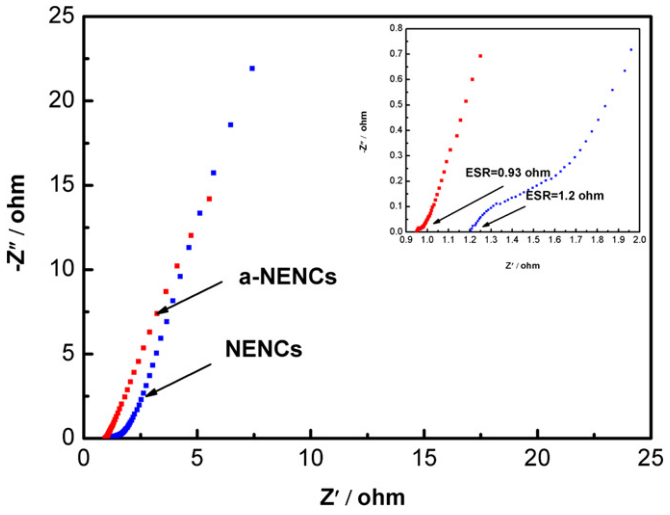

Fig. 8. Nyquist plot based on the NENCs and a-NENCs electrodes with the frequency range of 10^5–10^{-2} Hz (the inset shows the expanded high-frequency region of the plot).

transfer resistance (R_{ct}) is extremely low from the inconspicuous semicircle of the a-NENCs electrodes (Fig. 8 insert). The results demonstrate that the a-NENCs possess excellent capacitive performance. This may be attributed to pseudo-Faradaic reactions involving the quinone functional groups [28].

Long cycle life of supercapacitor is paramount evaluation for practical applications. Fig. 9 reveals the change of specific capacitance versus cycle number for the a-NENCs at the constant charge/discharge current density of 500 mA g^{-1}. It can be found that the specific capacitances of the a-NENCs supercapacitor increase gradually at the beginning of cycles due to an initial activation process for Faradaic pseudocapacitance of the materials. Then, the value of the specific capacitance reaches 89.5 F g^{-1}, it fluctuates a little, which is attributed to the instability of the functional groups. Finally, there is a slight decrease after 1500 cycles, but the specific capacitance maintains at a stable value till 2500 cycles. In addition, the Coulombic efficiency (charge capacitance/discharge capacitance) remains at 100% during the cycling process. So it is believed that the a-NENCs have much better electrochemical performance and will be a potential active material for the application of supercapacitor.

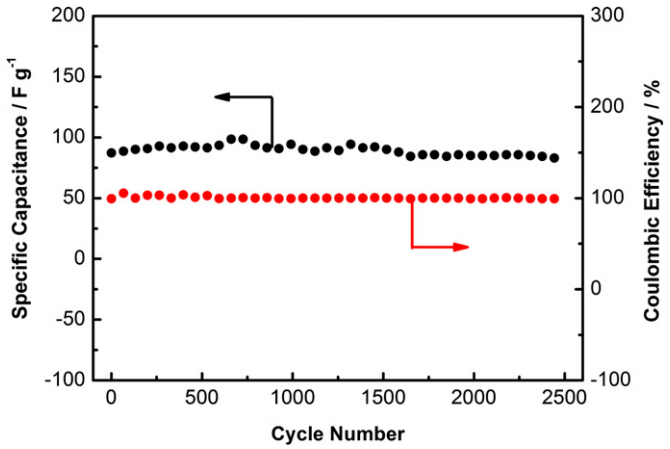

Fig. 9. Charge/discharge cycle (2500 cycles) of the a-NENCs supercapacitor at a current density of 500 mA g^{-1}: discharge capacitance (●) and Coulombic efficiency (●).

4. Conclusion

The nitrogen-enriched carbon materials (NENCs) have been obtained by the carbonization of the PANI/ACMB composites at 600 °C for 2 h in Ar atmosphere and following activated by 16 M HNO_3, which will keep the leechee-like morphology of the original PANI/ACMB. The maximum specific capacitance of the electrode is as high as 385 F g^{-1} at a current density of 1 A g^{-1} in 6 M KOH electrolyte by galvanostatic charge/discharge measurement. Meanwhile, the a-NENCs have small equivalent series resistance and the value is only 0.93 Ω. Moreover, the a-NENCs possess excellent stability and reversibility, the specific capacitance of the button supercapacitor is as high as 89.5 F g^{-1} and the Coulombic efficiency remains at 100% during the cycling process. The good electrochemical performance of the a-NENCs is ascribed to well-developed micropores (less than 1.3 nm) in the a-NENCs, the presence of functional groups generating the Faradaic pseudocapacitance and low equivalent series resistance. Therefore, the a-NENCs will be a kind of potential electrode active materials for the application of the high performance supercapacitors.

Acknowledgments

This work was financially supported by the National Natural Science Foundation of China (Grant Nos. 51272221, 51072173 and 21203161), Specialized Research Fund for the Doctoral Program of Higher Education (Grant No. 20094301110005).

References

[1] Y.P. Zhai, Y.Q. Dou, D.Y. Zhao, P.F. Fulvio, R.T. Mayes, S. Dai, Adv. Mater. 23 (2011) 4828–4850.
[2] K. Kierzek, E. Frackowiak, G. Lota, G. Gryglewicz, J. Machnikowski, Electrochim. Acta 49 (2004) 515–523.
[3] W. Li, G. Reichenauer, J. Fricke, Carbon 40 (2002) 2955–2959.
[4] X. Yan, H.H. Song, X.H. Chen, J. Mater. Chem. 19 (2009) 4491–4494.
[5] L.L. Zhang, X.S. Zhao, Chem. Soc. Rev. 38 (2009) 2520–2531.
[6] E. Frackowiak, Phys. Chem. Chem. Phys. 9 (2007) 1774–1785.
[7] A.G. Pandolfo, A.F. Hollenkamp, J. Power Sources 157 (2006) 11–27.
[8] D. Hulicova, J. Yamashita, Y. Soneda, H. Hatori, M. Kodama, Chem. Mater. 17 (2005) 1241–1247.
[9] N.D. Kima, W.Y. Kima, J.B. Joo, S. Oh, P. Kimb, Y.H. Kim, J.H. Yi, J. Power Sources 180 (2008) 671–675.
[10] C. Vagner, G. Finqueneisel, T. Zimmy, P. Burg, B. Grzyb, J. Machnikowski, J.V. Weber, Carbon 41 (2003) 2847–2853.
[11] D.S. Yuan, T.X. Zhou, S.L. Zhou, W.J. Zou, S.S. Mo, N.N. Xia, Electrochem. Commun. 13 (2011) 242–246.
[12] D. Hulicova, M. Kodama, H. Hatori, Chem. Mater. 18 (2006) 2318–2326.
[13] C. Wu, X.Y. Wang, B.W. Ju, X.Y. Zhang, L.L. Jiang, H. Wu, Int. J. Hydrogen Energy 37 (2012) 14365–14372.
[14] J.H. Kim, Y.S. Lee, A.K. Sharma, C.G. Liu, Electrochim. Acta 52 (2006) 1727–1732.
[15] X.F. Lu, H. Mao, W.J. Zhang, Polym. Compos. 30 (2009) 847–854.
[16] J.J. Xu, K. Wang, S.Z. Zu, B.H. Han, Z.X. Wei, ACS Nano 4 (2010) 5019–5026.
[17] A. Janošević, G. Ćirić-Marjanović, B. Marjanović, P. Holler, M. Trchová, J. Stejskal, Nanotechnology 19 (2008) 135606–135614.
[18] M. Trchová, I. Šeděnková, E.N. Konyushenko, J. Stejskal, P. Holler, G. Ćirić-Marjanović, J. Phys. Chem. B 110 (2006) 9461–9468.
[19] G. Ćirić-Marjanović, V. Dondur, M. Milojević, M. Mojović, S. Mentus, A. Radulović, Z. Vuković, J. Stejskal, Langmuir 25 (2009) 3122–3131.
[20] T. Maiyalagan, B. Viswanathan, Mater. Chem. Phys. 93 (2005) 291–295.
[21] X. Wang, N. Liu, W. Zhang, Y. Wei, Chem. Lett. 34 (2005) 42–43.
[22] M. Trchová, P. Matějka, J. Brodinová, A. Kalendová, J. Prokeš, J. Stejskal, Polym. Degrad. Stab. 91 (2006) 114–121.
[23] S. Biniak, G. Szymański, J. Siedlewski, A. Swiatkowski, Carbon 35 (1997) 1799–1810.
[24] T.E. Rufford, D. Hulicova-Jurcakova, Z.H. Zhu, G.Q. Lu, Electrochem. Commun. 10 (2008) 1594–1597.
[25] Y.J. Kim, Y. Abe, T. Yanagiura, K.C. Park, M. Shimizu, T. Iwazaki, S. Nakagawa, M. Endo, M.S. Dresselhaus, Carbon 45 (2007) 2116–2125.
[26] R. Pietrzak, Fuel 88 (2009) 1871–1877.
[27] K.S. Xia, Q.M. Gao, J.H. Jiang, J. Hu, Carbon 46 (2008) 1718–1726.
[28] X.X. Xiang, E.H. Liu, L.M. Li, Y.J. Yang, H.J. Shen, Z.Z. Huang, Y.Y. Tian, J. Solid State Electrochem. 15 (2011) 579–585.
[29] J.P. Yang, Y.P. Zhai, Y.H. Deng, D. Gu, Q. Li, Q.L. Wu, Y. Huang, B. Tu, D.Y. Zhao, J. Colloid Interf. Sci. 342 (2010) 579–585.
[30] B. Xu, F. Wu, D. Mu, L. Dai, G. Cao, H. Zhang, Int. J. Hydrogen Energy 35 (2010) 632–637.
[31] C.C. Hu, C.C. Wang, Electrochem. Commun. 4 (2002) 554–559.
[32] H. Teng, Y.J. Chang, C.T. Hsieh, Carbon 39 (2001) 1981–1987.
[33] Y.G. Wang, H.Q. Li, Y.Y. Xia, Adv. Mater. 18 (2006) 2619–2623.
[34] D.Y. Qu, J. Power Sources 109 (2002) 403–411.
[35] B.E. Conway, Electrochemical Supercapacitors: Scientific Fundamentals and Technological Applications, Kluwer Academic/Plenum Publishers, New York, 1999.
[36] A. Burke, J. Power Sources 91 (2000) 37–50.
[37] A. Nishino, J. Power Sources 60 (1996) 137–147.